MODELING CRACK GROWTH WITH SELECTIVELY ACTIVATED COHESIVE ELEMENTS

William M. Peterson, Douglas S. Cairns
Montana State University
Bozeman MT, 59717

ABSTRACT

Fracture simulations in 2D are performed to evaluate the effect of multiple material flaws without predefining the fracture path. The use of a modified cohesive zone model is demonstrated, in which cohesive interface elements are initially placed at inter-element boundaries throughout a finite element mesh, but remain dormant until selectively reactivated only where needed during the course of an analysis. Prior to the onset of damage, interfacial separation is prevented by using controllable master-slave multipoint constraints which eliminate slave degrees of freedom from the system. Once reactivated, subsequent inter-element separation and damage evolution may proceed using an appropriate extrinsic traction-separation law, where the initial cohesive tractions are based on averaged border element stresses at the interface. Selective activation successfully alleviates the problem of artificial added compliance inherent to the intrinsic approach, while activating additional degrees of freedom only as needed to permit crack growth without the need for adaptive remeshing operations. The method is implemented as a user-element subroutine (UEL) in the FEM code Abaqus/Standard using a formulation that provides solution values from the continuum "border" elements on either side of the interface in each current iteration in a fully implicit manner.

1. INTRODUCTION

Material fracture and failure may be represented by the cohesive zone model (CZM), in which internal cohesive forces resist material separation across an extended crack tip [1,2,3]. The crack opening is generally governed by a traction-separation law (TSL) that defines the development of cohesive tractions across an interface as a function of the interfacial separation, leading to failure of the material. The CZM is implemented in the finite element method using zero-thickness cohesive interface elements (CIEs) placed within the mesh between standard continuum elements, thereby forming a path through which cracks may propagate by permitting local displacement jumps at the inter-element boundaries.

In practice, CIEs are often placed within the mesh along an expected fracture path. For example, CIEs may be placed at ply boundaries in order to study the delamination of composite laminates [4]. In such cases the CIE exhibits an initial elastic response prior to the onset of damage. Once a damage criterion has been satisfied, the cohesive TSL is generally defined in order to describe the irreversible loss of stiffness until failure of the material occurs. Because the CIEs exist within the mesh prior to obtaining the solution, this approach has become known as the intrinsic CZM.

Alternatively, CIEs may be inserted between all elements within a region of interest so that each inter-element boundary becomes a potential fracture path [5,6]. The main advantage of the "full" intrinsic CZM is that neither an initial crack nor the fracture path must be predefined. Multiple cracks, crack interaction, and fragmentation are naturally permitted to occur at any location within

the mesh. However, despite this versatility the full intrinsic model is apparently absent from commercial finite element codes and is not commonly seen in the literature. This is perhaps due to a few shortcomings of the intrinsic approach, which include (1) an artificial added compliance of the model due to the necessity of an initial elastic response, (2) the large number of additional degrees of freedom (DOF) that result during mesh splitting and CIE insertion, and (3) the potential fracture paths are limited to inter-element boundaries. In many cases, the artificial compliance induced by the finite initial stiffness of the intrinsic TSL is the most difficult to overcome. To compensate, the analyst may choose to reduce artificial compliance by assuming very large values for the initial elastic "penalty" stiffness, such that the interface becomes nearly rigid prior to the onset of damage and softening. Unfortunately, this leads to ill-conditioning of the global system of equations and numerical non-convergence. In practice, a suitable value for the penalty stiffness in intrinsic models is usually only found by iteration, which further increases the total cost of the analysis. Crack growth mesh dependence may also be acceptably reduced by using a sufficiently refined and unstructured mesh which provides a variety of potential fracture paths, and then performing a parametric study over a reasonable number of mesh variants. As is often the case, there is a trade-off between acceptable computational expense and accuracy.

In a second approach referred to as an initially-rigid or extrinsic cohesive model, CIEs are adaptively inserted wherever required as the solution progresses [7]. This approach reduces the issue of artificial compliance, while preventing CIE insertion and the corresponding increase in the number of active DOF in parts of the mesh where damage is not indicated. Unfortunately, continual remeshing operations are often computationally inefficient and tend to require sophisticated data storage and transfer routines.

2. A SELECTIVELY ACTIVATED COHESIVE ZONE MODEL

In this section a new approach is described that combines advantages of both intrinsic and extrinsic models by a method of selective activation.

2.1 Mesh Splitting and Cohesive Element Insertion

Similar to the intrinsic approach, in the selectively activated CZM cohesive elements are inserted at every inter-element boundary found within the initial mesh during model preprocessing. This has been accomplished by using a fast and robust in-house remeshing code specifically developed for this purpose, which operates on the standard nodal coordinate and element connectivity tables that are commonly produced by finite element mesh generators. The process begins by separating each element in the mesh from all adjacent elements, forming a domain of fully discontinuous elements with unique nodes and surfaces. Each original "parent" node is duplicated as many times as it is shared by elements in the original mesh, and each new "child" node shares the exact location in space as the parent node. Zero-thickness CIEs are then inserted at all inter-element boundaries. Once CIE insertion is complete a full intrinsic CZM has been generated, as shown in Fig. 1. Note that in many practical fracture analyses this process results in a substantial increase in the number of nodes and associated DOF.

2.2 Application of Multi-Point Constraints

Using element adjacency information obtained during the remeshing step, node-to-node linear master-slave multi-point constraints (MPCs) are defined such that the superposed nodes of adjacent elements are exactly constrained to prevent relative displacements via a congruent

transformation (Fig. 2). The eliminated slave DOF are retained so that they may be reactivated as needed during the analysis; however, the number of active DOF on the new mesh is equal to that of the original mesh by virtue of the method. Thus, each intrinsic cohesive element enters a "dormant" state and has no effect on the response of the structure.

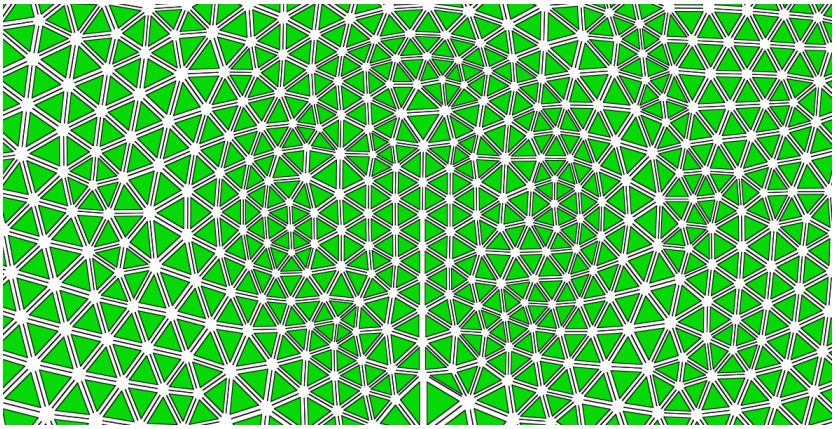

Figure 1: Example intrinsic CZM mesh. Continuum elements are shrunk in order to clarify the position of the inserted CIEs. Note the crack at the center, where CIEs are not present.

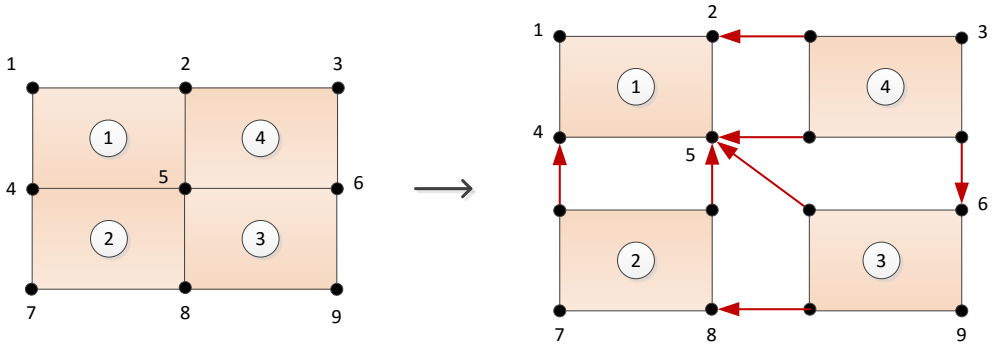

Figure 2: Illustration of mesh splitting and application of node-to-node multipoint constraints. The location of the original nodes are also shown on the split mesh. Note that retaining the original nodes as master nodes, in their original location, simplifies the transfer of boundary conditions defined on the original mesh.

During the analysis, at the conclusion of each converged increment the solution is investigated to identify critical regions in the mesh. Constraints may then selectively deactivated wherever a damage criterion is satisfied. Subsequent inter-element displacement and damage evolution is then governed by an appropriate TSL. In other words, the solution continues to the next increment without interruption even as cohesive elements and DOF are reintroduced into the model.

The proposed model has been implemented via a user subroutine coupled with the commercial finite element code Abaqus/Standard (implicit) [8]. The MPC, UFIELD, and UEL subroutines allow access to certain key functionalities. Additional access to shared variables that cannot

otherwise be communicated through the subroutine arguments is provided through a Fortran Module.

2.3 Patch Test Comparison

In the following section, the 2D finite element patch test is adapted in order to illustrate the differences between a conventional mesh using continuum elements only, an intrinsic CZM, and the selectively activated MPC-based cohesive zone model, denoted here as the MCZM. This example serves to clearly demonstrate that even using very large initial penalty stiffness values, K, the intrinsic CZM fails to calculate the correct displacement solution; consequently, the use of a large penalty value for K will fail to preserve the correct element-local response (for example, the stress in the element) in the intrinsic model.

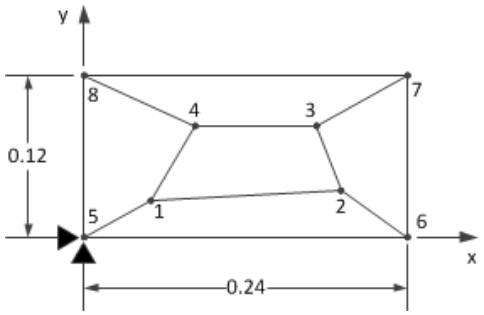

Figure 3. Typical 5-element membrane patch test. All units in meters

Consider the 5-element membrane 2D patch test in Fig. 3, adapted from [8]. The mesh shown consists of linear plane-strain elements where the Young's modulus and Poisson's ratio are E=1.0 MPa and ν= 0.25. All exterior nodes (Nodes 5-8) are subjected to the prescribed displacement field:

$$U_x = 10^{-3}(x + 0.5y) \tag{1a}$$

$$U_y = 10^{-3}(0.5x + y) \tag{1b}$$

Therefore, the boundary conditions at the exterior nodes are:

Node 5:	$U_x = 0$	$U_y = 0$
Node 6:	$U_x = 0.24 \cdot 10^{-3} m$	$U_y = 0.12 \cdot 10^{-3} m$
Node 7:	$U_x = 0.3 \cdot 10^{-3} m$	$U_y = 0.24 \cdot 10^{-3} m$
Node 8:	$U_x = 0.06 \cdot 10^{-3} m$	$U_y = 0.12 \cdot 10^{-3} m$

For a mesh of linear elements, the patch test is passed if the displacement of the interior nodes (Nodes 1-4) match the prescribed displacement field given in Eq. (1). The analytical reference solution for the displacement of the interior nodes is:

Node 1:	$U_x = 0.05 \cdot 10^{-3} m$	$U_y = 0.04 \cdot 10^{-3} m$

Node 2:	$U_x = 0.195 \cdot 10^{-3} m$	$U_y = 0.12 \cdot 10^{-3} m$
Node 3:	$U_x = 0.2 \cdot 10^{-3} m$	$U_y = 0.16 \cdot 10^{-3} m$
Node 4:	$U_x = 0.12 \cdot 10^{-3} m$	$U_y = 0.12 \cdot 10^{-3} m$

In Fig. 4, the construction and final active DOF for each model is illustrated. Results from several different intrinsic CZM models with increasing penalty stiffness values are provided in Table 1. Note that the cohesive element stiffness chosen for the MCZM is arbitrary for this example, since the CIEs are effectively condensed from the problem and the MPCs are not released. The displacement field plots for example solutions are shown in Figs. 5-8. Note that for clarity, the cohesive elements are not visualized. From these figures, it is clear that the conventional and MCZM meshes pass the displacement patch test. Note that displacement continuity must necessarily be exactly satisfied using the master-slave MPC approach. On the other hand, the intrinsic cohesive mesh exhibits severe displacement discontinuities, even without permitting damage initiation and for very high penalty stiffness.

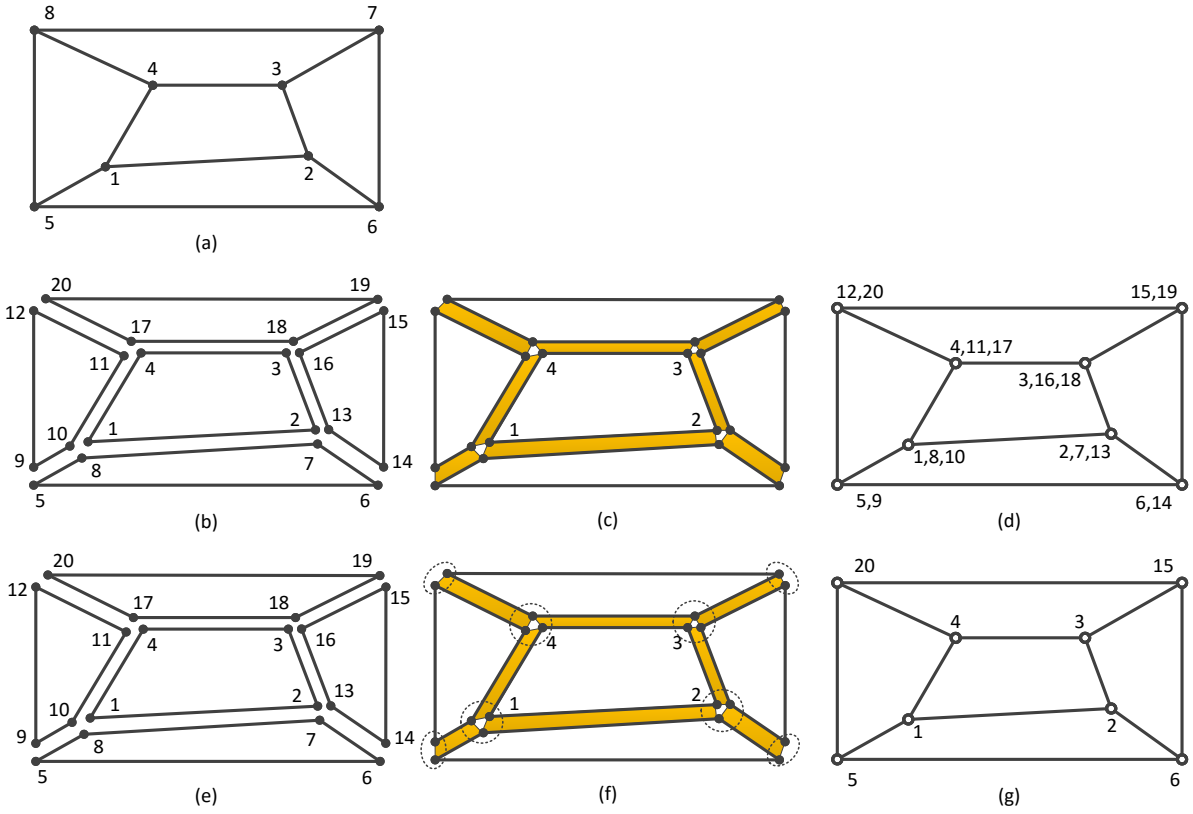

Figure 4. Construction of patch test models. Top (a): conventional mesh; Middle (b-c): intrinsic CZM; Bottom (e-f): MCZM. Gaps between elements are shown only for clarity. Cohesive elements are shaded. Only nodes with active DOF are numbered by the right-most figure in each row. Note that the interior element has the same nodal numbering in each model.

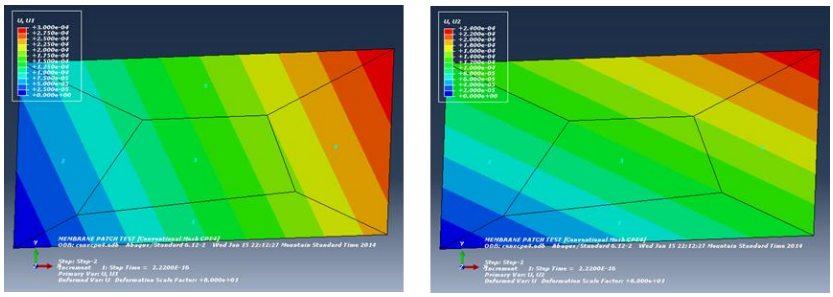

Figure 5. Conventional mesh patch test: displacement. Left: U1, right: U2. Scale factor=80.

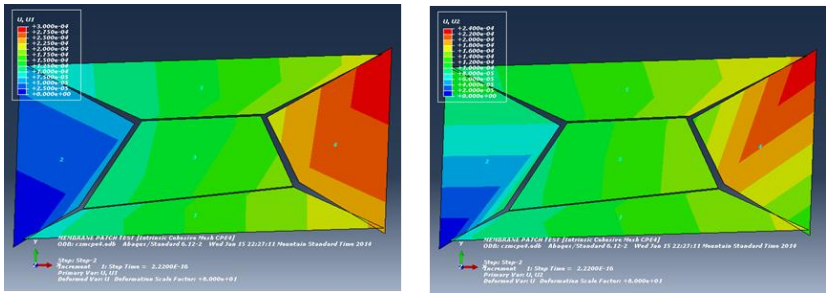

Figure 6. Intrinsic mesh (K=10·E) patch test: displacement. Left: U1, right: U2. Scale factor=80.

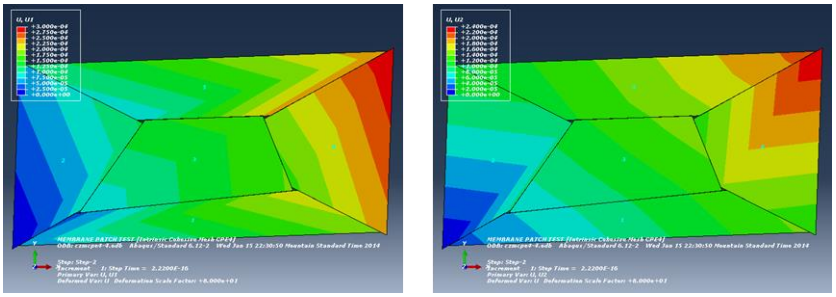

Figure 7. Intrinsic mesh (K=10^4·E) patch test: displacement. Left: U1, right: U2. Scale factor=80.

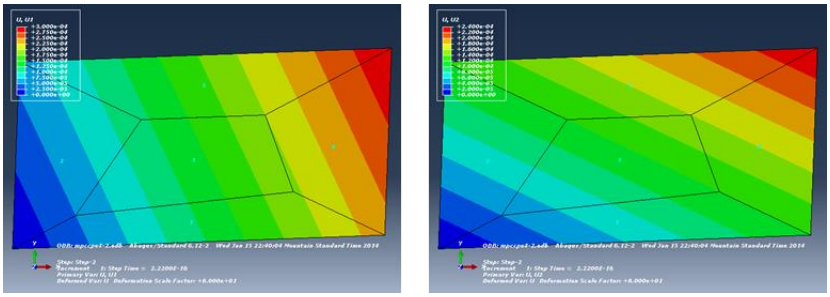

Figure 8. MCZM patch test: displacement. Left: U1, right: U2. Scale factor=80.

Table 1. Models used in the patch test comparison

#	Model Description	Penalty Stiffness, *K*

1	Conventional (Linear Plane Strain CPE4) Mesh	NA
2	Intrinsic Cohesive Mesh	$10^{1} \cdot E$
3	Intrinsic Cohesive Mesh	$10^{2} \cdot E$
4	Intrinsic Cohesive Mesh	$10^{3} \cdot E$
5	Intrinsic Cohesive Mesh	$10^{4} \cdot E$
6	MCZM	$10^{1} \cdot E$

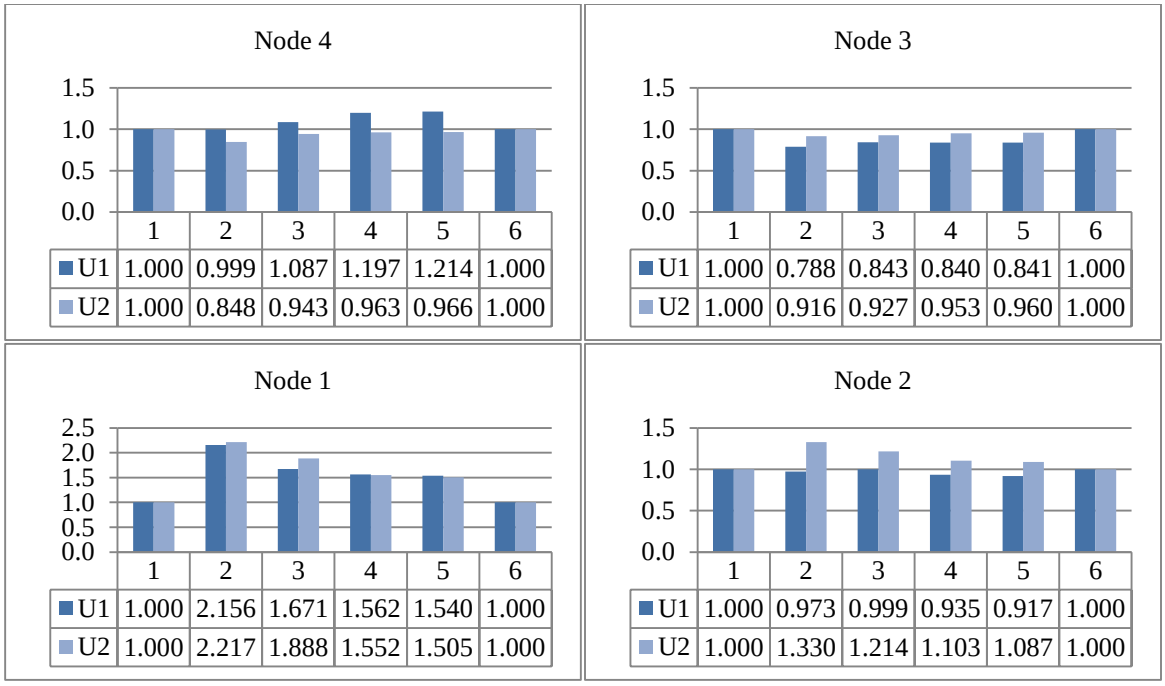

Figure 9: Displacement solution at nodes 1-4 of the interior element, normalized to the analytical solution. Note that an exact solution is represented by a value of "1.0". See Table 1 for a description of Models 1-6.

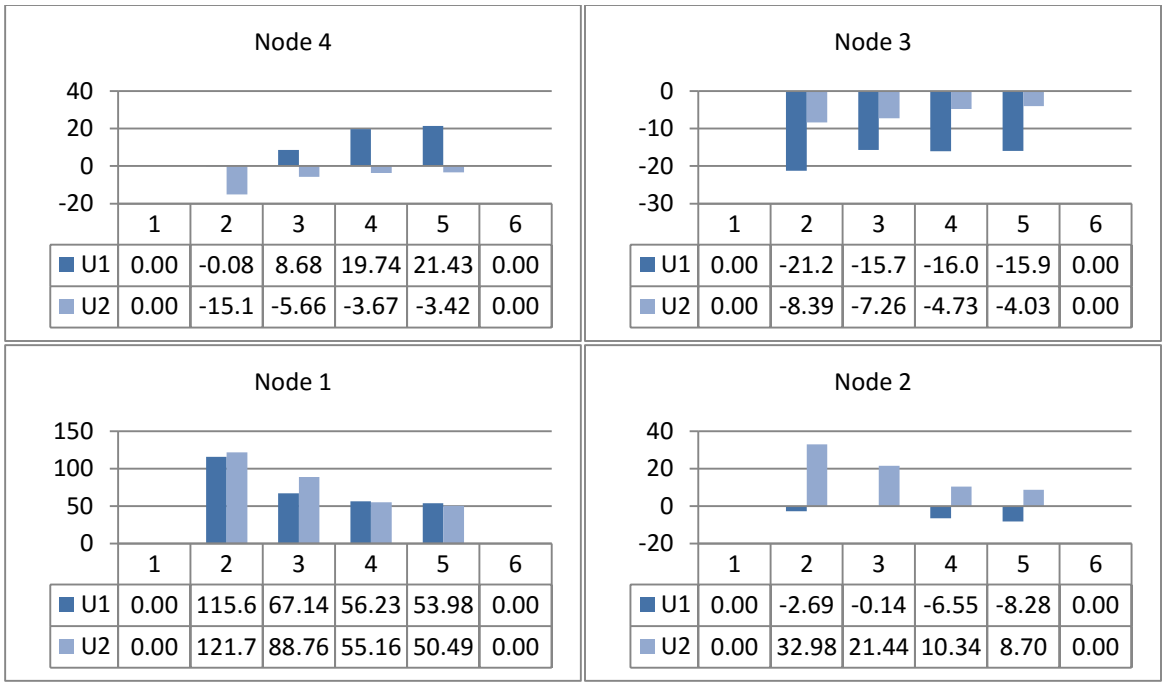

Figure 10: Percent error in the displacement solution at nodes 1-4 of the interior element. Note that an exact solution is represented by a value of '0'. See Table 1 for description of Models 1-6.

In Fig. 9, the displacements of the interior nodes are shown, normalized to the exact solution. Nodes are numbered as shown in Fig. 4, and models 1-6 are described in Table 1. It can be seen that the conventional and MCZM meshes arrive at the correct values, while the intrinsic mesh fails to reach the correct local solution even for very large penalty stiffness, K. It can also be seen that as K increases (by 4 orders of magnitude), there does not appear to be any general improvement in the solution computed with the intrinsic mesh. This is perhaps made more evident in Fig. 10, where the percent errors for the interior node displacements are shown.

3. DRILLED PLATE VALIDATION TEST

An interesting problem by Ingraffea and Grigoriu [9], similar to that of Bittencourt et al. [10], is taken as a test of the selectively activated CZM. In their work, Plexiglas (PMMA) specimens were tested in 3-point bending under the influence of three drilled holes, and the resulting crack path was investigated for various initial crack locations and lengths. Here, only one of the crack geometries used by them is discussed, and the resulting fracture path is determined for three values of the cohesive fracture energy, G_{crit}. A simple displacement-controlled boundary condition was applied to the center of the top edge. The geometry and isotropic material properties are illustrated in Fig. 11. A standard 2D cohesive element available in Abaqus was used without modification of the intrinsic TSL with an initial stiffness of $10 \cdot E$ (in a future publication an alternative UEL-based cohesive element with an extrinsic TSL will be demonstrated). Multipoint constraints were released at an effective Mises stress of $\sigma_{rel} = 0.95 * \sigma_{max}$. The mesh consisted of 58875 nodes with 19625 3-node linear triangles (CST) and 29223 4-node bilinear cohesive elements. Solutions were

obtained between 45-60 mins using 2 cores on a modest Intel i3 with 6GB RAM running Windows 7.

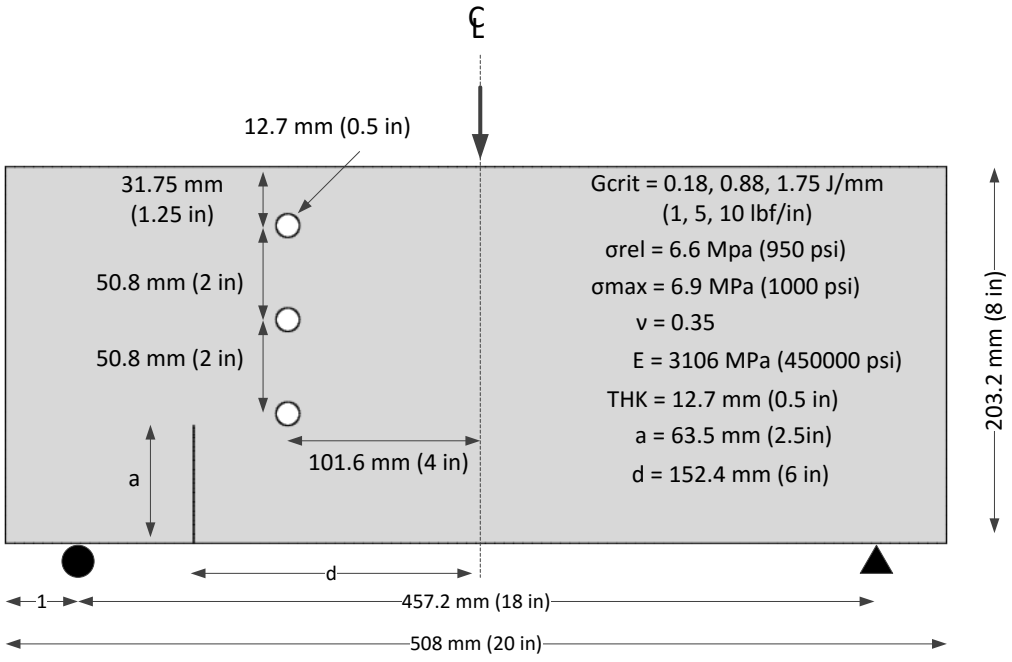

Fig. 11: Ingraffea/Bittencourt's Drilled Plate [9,10].

The crack paths are shown in Figs. 12-14. Dark lines or dots on the interior of the model indicate the presence of a free surface – i.e. an MPC has been released. The results are encouraging, although not exactly the same as in [9]. This discrepancy is partly due to the restriction that crack growth must occur along inter-element boundaries, and partly a result of the simple displacement control method used in this analysis. To illustrate the effects of uncertainty in the fracture energy (G_{crit}), for the same mesh the change in the crack path as the critical fracture energy increases is shown.

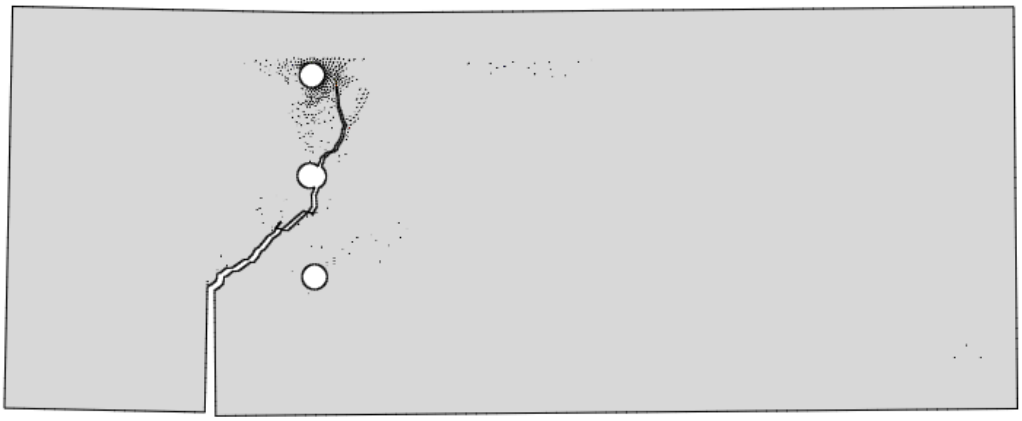

Fig. 12: Selectively Activated CZM; G_{crit} = 1.75 N/mm (10 lbf/in). Scale factor=1.

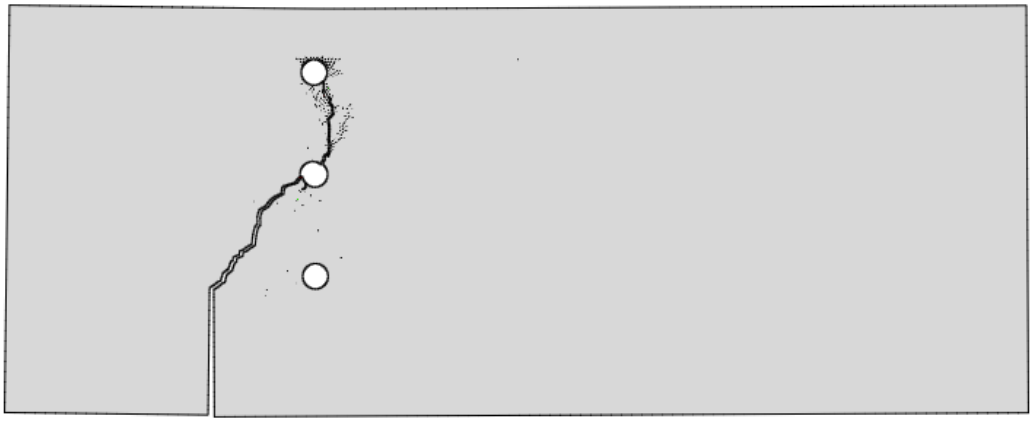

Fig. 13: Selectively Activated CZM; G_{crit} = 0.88 N/mm (5 lbf/in). Scale factor=1.

Fig. 14: Selectively Activated CZM; G_{crit} = 0.175 N/mm (1 lbf/in). Scale factor=1.

4. CONCLUSIONS

The cohesive zone model is a versatile tool for modeling crack initiation and propagation under complex loading conditions, but both intrinsic and extrinsic approaches suffer from some drawbacks. The selective activation of intrinsic cohesive elements appears to be a natural extension that removes or lessens these issues by (1) alleviating the effect of artificial compliance, (2) minimizing the number of DOF in the system matrix while retaining eliminated DOF for reactivation as needed, and (3) utilizing dormant cohesive elements that are selectively reactivated at inter-element boundaries only as needed by the analysis, rather than by interrupting the solution in order to perform adaptive remeshing and element insertion. The method is quite flexible, as well, permitting the reactivation of MPCs upon sufficient relaxation of the undamaged CIEs in a cohesive zone after a crack has passed through a formerly critical region. Continued development will be reported in future publications.

5. REFERENCES

1. Barenblatt, G, “The mathematical theory of equilibrium cracks in brittle fracture”, Advances in Applied Mechanics, Vol. 7, 1962, pp. 55-129.
2. Dugdale, D., “Yielding of steel sheets containing slits”, Journal of the Mechanics and Physics of Solids, Vol. 8, 1960, pp. 100-104.
3. Hillerborg, A., Modeer, M. and Petersson, P., “Analysis of crack formation and crack growth in concrete by means of fracture mechanics and finite elements”, Cement and Concrete Research, Vol. 6, 1976, pp. 773-782.
4. Alfano, G., and Crisfield, M.A., “Finite element interface models for the delamination analysis of laminated composites: mechanical and computational issues”, International Journal for Numerical Methods in Engineering, Vol. 50, 2001, pp. 1701-1736.
5. Ortiz, M., and Suresh, S., “Statistical properties of residual stresses and intergranular fracture in ceramic materials”, Journal of Applied Mechanics, Vol. 60, 1993, pp. 77-84.
6. Xu, X.-P, and Needleman, A., “Numerical simulations of fast crack growth in brittle solids”, Journal of the Mechanics and Physics of Solids, Vol. 42, 1994, pp. 1397-1434.
7. Camacho, G. T.; Ortiz, M., “Computational modelling of impact damage in brittle materials”, International Journal of Solids and Structures, 1996, Vol. 33; pp. 2899-2938.
8. Abaqus User’s Manual, Ver. 6.12, SIMULIA, 2012.
9. Ingraffea, A.R; Grigoriu, M., “Probabilistic fracture mechanics; A validation of predictive capability”, AFOSR Final Report, 1990.
10. Bittencourt, T.N.; Wawrzynek, P.A.; Ingraffea, A.R.; “Quasi-automatic simulation of crack propagation for 2D LEFM problems”, Engineering Fracture Mechanics, 1995, Vol. 55, No. 2; pp. 321-334.